Atmospheric, radiative, and hydrologic effects of future land use and land cover changes: A global and multimodel climate picture

Benjamin Quesada, Almut Arneth, Nathalie de Noblet-Ducoudré

AGU PUBLICATIONS

JGR

Journal of Geophysical Research: Atmospheres

RESEARCH ARTICLE
10.1002/2016JD025448

Key Points:
- A large panel of future biophysical effects of land use and land cover changes (LULCC) is assessed and quantified in a multimodel framework
- Future LULCC weaken the hydrological cycle and reveal a positive tropical soil-moisture/precipitation feedback after deforestation
- Indirect atmospheric feedback can dominate over direct effects to explain simulated climatic changes

Supporting Information:
- Supporting Information S1

Correspondence to:
B. Quesada,
benjamin.quesada@kit.edu

Citation:
Quesada, B., A. Arneth, and N. de Noblet-Ducoudré (2017), Atmospheric, radiative, and hydrologic effects of future land use and land cover changes: A global and multimodel climate picture, *J. Geophys. Res. Atmos.*, *122*, 5113-5131, doi:10.1002/2016JD025448.

Received 31 MAY 2016
Accepted 26 APR 2017
Accepted article online 28 APR 2017
Published online 17 MAY 2017

Atmospheric, radiative, and hydrologic effects of future land use and land cover changes: A global and multimodel climate picture

Benjamin Quesada[1], Almut Arneth[1], and Nathalie de Noblet-Ducoudré[2]

[1]Institute of Meteorology and Climate Research, Atmospheric Environmental Research, Karlsruhe Institute of Technology, Garmisch-Partenkirchen, Germany, [2]Laboratoire des Sciences du Climat et de l'Environnement LSCE/IPSL, Unité mixte CEA-CNRS-UVSQ, Université Paris Saclay, Gif-sur-Yvette, France

Abstract Land use and land cover changes (LULCC) modulate land surface energy, heat, moisture, and momentum fluxes. Using simulations performed with and without LULCC for five earth system models, averaged over the 2071–2100 period, we quantify the biophysical effects in response to a future realistic LULCC scenario (Representative Concentration Pathway RCP8.5) on 15 climate variables (i.e., atmospheric, radiative, wind, hydrologic variables, and heat fluxes). We find that climate models are able to simulate some robust and strong climate perturbations in response to LULCC. In tropical regions with substantial LULCC, significantly higher skin temperatures, less precipitation and soil moisture, less evaporation and clouds, more incoming radiation and stronger winds, more anticyclonic conditions and subsidence, are simulated in response to future LULCC. In midlatitude and high latitude, LULCC result in autumn cooling and higher tropospheric pressures, while East Asia is drier, warmer, with higher sensible heat flux and lower evaporation. The tropical wind strengthening and weakening of the hydrological cycle are comparable in magnitude to their future regional changes induced by greenhouse gases under RCP8.5, which make LULCC an indispensable forcing to take into account in future climatic assessments. Finally, our study reveals significant indirect atmospheric processes triggered by LULCC, implying substantial changes in incoming radiation, which dominate climatic responses over the direct effects, particularly in boreal regions.

Plain Language Summary Trees affect climate not only by modulating greenhouse gases sequestration but also by regulating the exchange of energy, heat, water, and momentum with the atmosphere. However, few studies quantified, in a consistent way, all the latter perturbations for a realistic deforestation scenario or with several models. Analyzing five earth system models, for a common future business-as-usual land use and land cover changes (LULCC) scenario, we show that significant atmospheric, radiative, and hydrologic changes are robustly simulated. Among others, the weakened hydrological cycle and the wind strengthening due to tropical deforestation are comparable in magnitude to the projected changes induced by greenhouse gases. Our investigation also reveals significant indirect atmospheric processes triggered by LULCC, implying substantial changes in incoming radiation, which dominate climatic responses over the direct effects (albedo, evapotranspiration, or roughness changes), particularly in boreal regions. In consequence, LULCC are a critical forcing that needs to be taken into account for future climatic assessments.

1. Introduction

Land use and land cover changes (LULCC) through deforestation, reforestation, or conversion of natural vegetation occur principally for urbanization and agriculture. LULCC have a recognized effect on climate, both in terms of changes in the vegetation and soil carbon and nitrogen cycles (biogeochemical effects) and variations of the biophysical properties of the land cover like albedo, evapotranspiration efficiency, and roughness (biophysical effects, hereafter "BPH" effects) [*Pielke et al.*, 1998; *Betts*, 2000; *Bala et al.*, 2007; *Bathiany et al.*, 2010; *Anderson-Teixeira et al.*, 2012; *Mahmood et al.*, 2014]. BPH effects of LULCC have been studied in many observational and modeling studies (see reviews and references therein: *Pielke et al.* [2011], *Mahmood et al.* [2014], and *Bright* [2015]). With growing sophistication of the land component of global climate models, two categories of biophysical forcing mechanisms in response to LULCC can be identified: radiative forcing (through albedo changes) and nonradiative forcing (in response to changes in evapotranspiration efficiency and aerodynamic resistance) [e.g., *Davin and de Noblet-Ducoudré*, 2010;

Intergovernmental Panel on Climate Change (IPCC), 2013]. Overall, modeling studies agree that regional deforestation in boreal and temperate regions mainly increases the surface albedo (i.e., biophysical cooling), whereas deforestation in the tropics leads to a weakened latent heat flux from evapotranspiration (biophysical warming) [*Bonan et al.*, 1992; *Betts*, 2000; *Bathiany et al.*, 2010; *Pielke et al.*, 2011; *Mahmood et al.*, 2014; *Devaraju et al.*, 2015b; *Lawrence and Vandecar*, 2015]. When aggregated at global scale, model intercomparison exercises found that biophysical effects of historical LULCC [e.g., *Pitman et al.*, 2009] and future LULCC [*Brovkin et al.*, 2013] are globally not significant, with a large spread among models [*Boisier et al.*, 2012], while responses at the regional scale were significant [e.g., *Pitman et al.*, 2009; *Brovkin et al.*, 2013; *Boysen et al.*, 2014]. Modeling studies performing idealized large-scale LULCC have shown significant changes in the mean regional climate [*Pielke et al.*, 2011; *Mahmood et al.*, 2014; *Lawrence and Vandecar*, 2015]. Moreover, the latitudinal dependence of BPH seems to emerge as a key feature raised both by observational [*Lee et al.*, 2011; *Zhang et al.*, 2014; *Li et al.*, 2015; *Alkama and Cescatti*, 2016] and modeling studies [e.g., *Bala et al.*, 2007; *Davin and de Noblet-Ducoudré*, 2010; *Devaraju et al.*, 2015b; *Li et al.*, 2016; *Perugini et al.*, 2017].

Except for experiments in intercomparison exercises (e.g., model intercomparison projects Land-Use and Climate, IDentification of robust impacts LUCID and LUCID-Coupled Model Intercomparison Project Phase 5 (CMIP5)), modeling studies are either limited to one global climate model, to one idealized LULCC scenario (e.g., 50%/100% deforestation [*Davin and de Noblet-Ducoudré*, 2010; *Lejeune et al.*, 2014]) and/or focus on one key region (e.g., Amazon basin [see *Lejeune et al.*, 2014; *Lorenz and Pitman*, 2014; *Lawrence and Vandecar*, 2015, and references therein]), thereby possibly overestimating climatic responses or neglecting the intermodel response variability. Moreover, a large majority of these studies analyze chiefly temperature and precipitation changes [e.g., *Claussen et al.*, 2001; *Bala et al.*, 2007; *Pongratz et al.*, 2010; *Brovkin et al.*, 2013; *Boysen et al.*, 2014; *Devaraju et al.*, 2015a, 2015b], but the investigations of the perturbation of energy, heat, moisture, and momentum balances together are not widespread. Finally, feedbacks with the atmosphere triggered by LULCC and their influence on the local climatic changes are subject to debate [*Pielke et al.*, 2011; *Mahmood et al.*, 2014]. Thus, many questions remain open regarding the response of local, regional, and global climate to changes in biophysical surface properties induced by LULCC. Using data from LUCID-CMIP5 project, our study aims to provide a comprehensive analysis of BPH effects of future LULCC, calculating corresponding changes in temperature, precipitation, pressure and hydrological variables, radiative and heat fluxes, cloudiness, and winds. In this line, this study attempts to address the following questions:

1. What are the robust global and regional BPH effects simulated in response to future LULCC? Are they consistent with findings from previous regional studies?
2. What are the physical mechanisms behind simulated BPH changes?
3. Can we identify atmospheric feedback and/or remote effects in response to LULCC?

In section 2, we present the models and their simulations, together with the analysis carried out on the modeled outputs. Section 3 shows the results per atmospheric variable and notable climatic features. Readers should be aware that in this section, we mainly discuss the net responses to LULCC above substantial land used areas. This means that in the same region or latitudinal band where both afforestation and deforestation take place, we will analyze their combined influence on climate. However, to be able to compare our results with the existing literature and to highlight other robust features, we will also quantify the impacts resulting from either deforestation or afforestation in parts of the Discussion (section 4).

2. Methods

Results from the five earth system models (ESM) involved in both the Coupled Model Intercomparison Project Phase 5 (CMIP5) and LUCID-CMIP5 are considered: Canadian Earth System Model version 2 (CanESM2), Institut Pierre-Simon Laplace-Climate Model version 5A-low resolution (IPSL-CM5A-LR), Hadley Centre Global Environmental Model version 2 Earth System (HadGEM2-ES), Model for Interdisciplinary Research on Climate ESM (MIROC-ESM), and Max-Planck-Institut ESM low resolution (MPI-ESM-LR) (see Table 1, hereafter called "LUCID-CMIP5 models"). For each model, two sets of simulations are analyzed. The first set includes RCP8.5 simulations from CMIP5, corresponding to a Representative Concentration Pathway leading to a radiative forcing of 8.5 W/m^2 in 2100. In this scenario, cropland and pasture areas increase at the expense of forests (see tree fraction changes in Figure 1). Those changes are mostly driven by an increasing global population and food demand [*van Vuuren et al.*, 2011]. The second set includes L2A85 simulations

Table 1. Description of the Five CMIP5 Models Used in LUCID-CMIP5, Atmospheric Horizontal Resolution (Longitude × Latitude), and Standard Abbreviations of Climate Variables Used for the Analysis[a]

LUCID -CMIP5 Model Acronym	Model Resolution	Institute, Country	Variables													
			TS	TAS	PR	PSL	ZG	WAP	RSDS	RLDS	RSUS	RLUS	HFSS	HFLS	CLT	WSPD	MRSOS
CanESM2	2.8° × 2.8°	CCCMA, Canada	X	X	X	X	X	X	X	X	X	X	X	X	X	X	X
HadGEM2-ES	1.3° × 1.9°	MOHC/INPE, UK	X	X	X	X	X		X	X	X	X	X	X	X	X	X
IPSL-CM5A-LR	1.9° × 3.8°	IPSL, France	X	X	X	X	X	X	X	X	X	X	X	X	X	X	X
MIROC-ESM	2.8° × 2.8°	MIROC, Japan	X	X	X	X	X	X	X	X	X	X	X	X	X	X	X
MPI-ESM-LR	1.9° × 1.9°	MPI-M, Germany	X	X	X	X	X	X	X	X	X	X	X	X	X	X	

[a]A cross is shown when both RCP85 (RCP85 runs from CMIP5, with land use and land cover changes) and L2A85 (L2A85 runs from LUCID-CMIP5, without land use and land cover changes and prescribed CO_2 concentrations of RCP85) outputs were available.

performed within the framework of the LUCID-CMIP5 project. They correspond to runs with prescribed atmospheric CO_2 concentration and sea-surface temperatures (plus sea ice extent) from the RCP8.5 scenario but without any land use and land cover change (LULCC) after the year 2005. Future biophysical (BPH) effects due to LULCC are thus calculated from the difference between RCP8.5 and L2A85 (RCP8.5 minus L2A85) simulations averaged over the 2071–2100 period (30 years). Future "LULCC intensity" (or ΔTreeFrac) is hereafter defined for each model as the net tree fraction changes simulated (*treeFrac* CMIP5 variable) between the years 2100 and 2006.

Future LULCC is implemented in different ways among CMIP5 models (see Annexes and Table 2 of *Brovkin et al.* [2013]). In addition to anthropogenic land cover changes, HadGEM2-ES, MPI-ESM-LR, and MIROC-ESM models calculate vegetation distribution in response to climate change dynamically which is not the case for CanESM2 and IPSL-CM5A-LR. Interpretation of land use classes, crop, and pasture areas differs between the coupled models. A detailed description of land use change maps implementation, and harmonization of land use change scenarios can be found in *Brovkin et al.* [2013]. For the RCP8.5 scenario, tree fraction

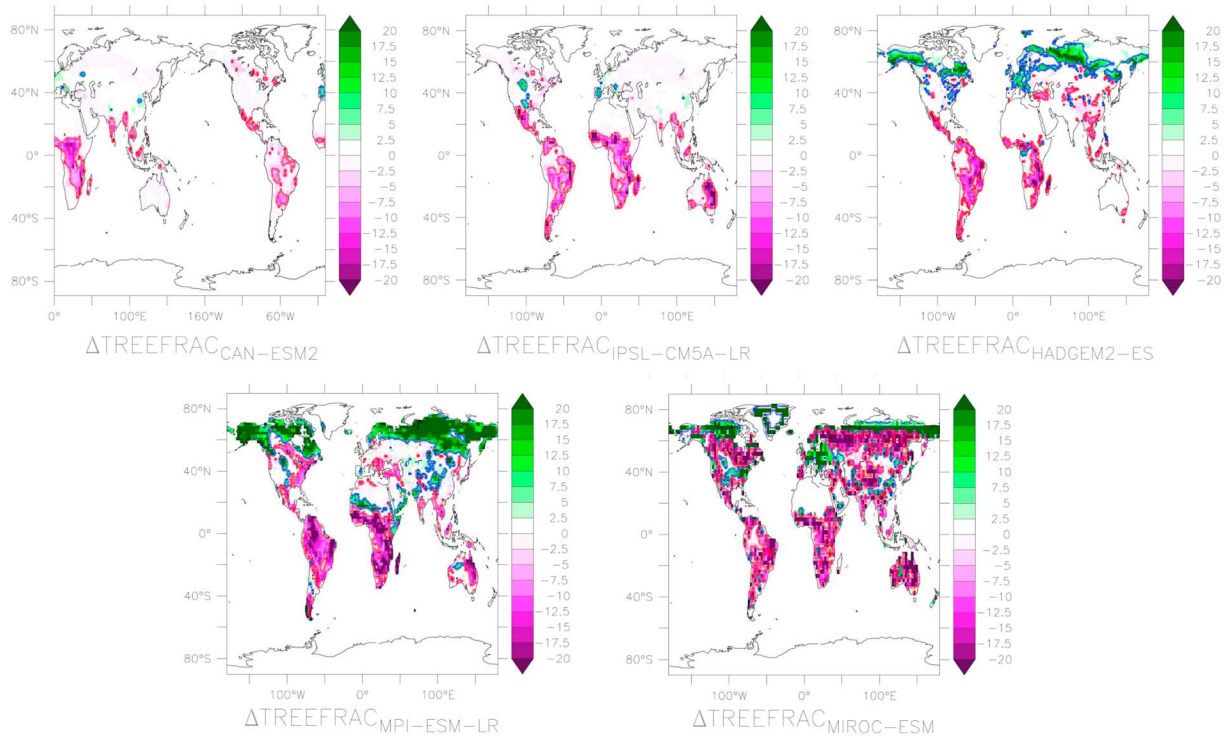

Figure 1. Tree fraction cover (%) changes for RCP8.5 scenario between years 2100 and 2006, as simulated by each of the 5 LUCID-CMIP5 models. The red (blue) contours are displayed for values less (greater) than −5% (5%).

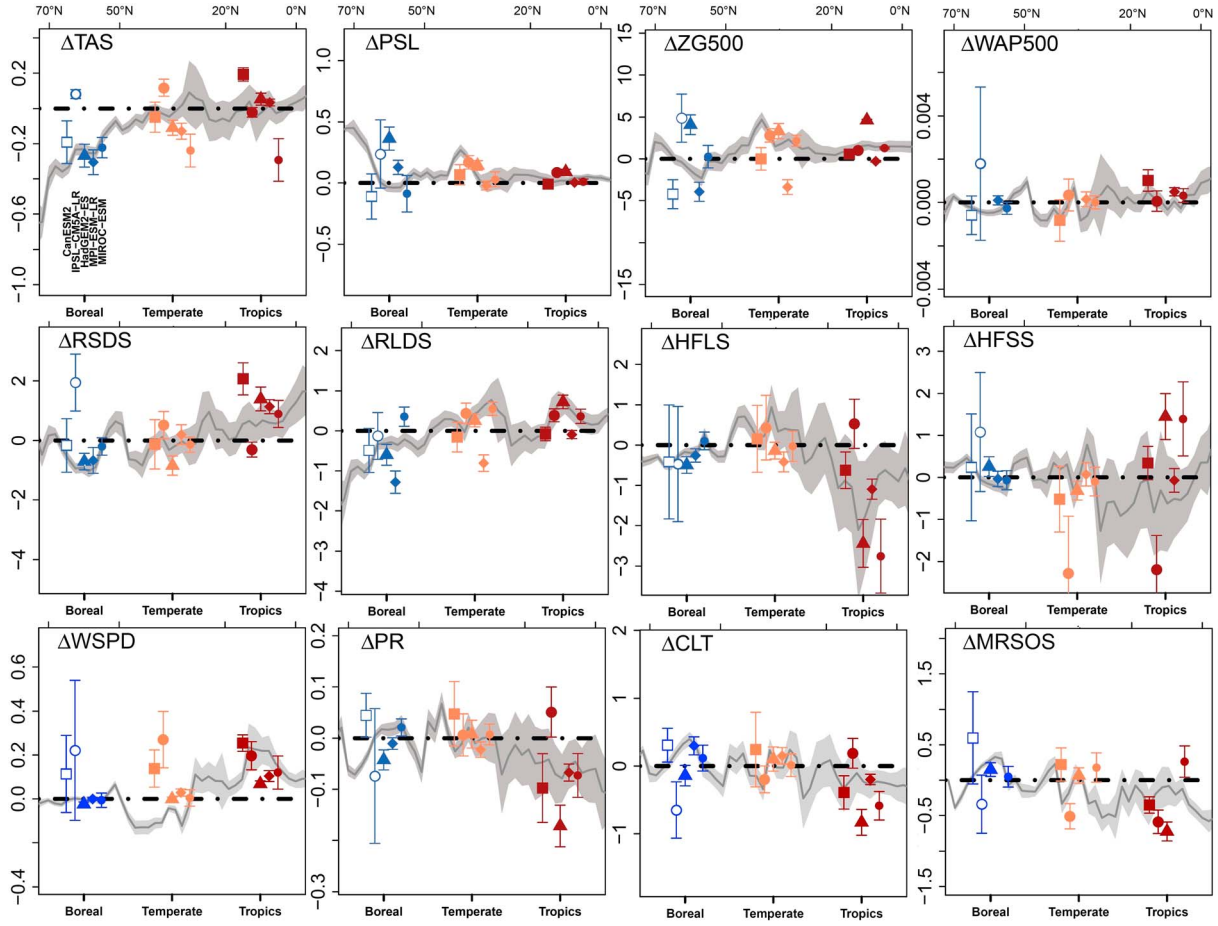

Figure 2. Simulated annual ENS-CMIP5 BPH changes in variables due to future LULCC in the boreal regions (blue), temperate regions (orange), or tropics (red), for the 2071–2100 period (under RCP8.5 scenario). Changes are averaged over grid points having experienced more than 5% change in tree fraction. Each symbol represents a model response and 95% confidence intervals calculated among grid cells of the same region (lower *x* axis). From left to right, symbols are for CanESM2, IPSL-CM5A-LR, HadGEM2-ES, MPI-ESM-LR, and MIROC-ESM. The empty (filled) symbols indicate model regional values obtained on less (more) than 50 gridcells satisfying the $|\Delta\text{TreeFrac}| > 5\%$ threshold (see Table S1). The grey line represents the zonal ensemble-mean averages (based on upper *x* axis from 0°N to 70°N) calculated over grid points with $|\Delta\text{TreeFrac}| > 5\%$ and the envelope the corresponding 95% confidence intervals calculated among all the latitudinal grid points of the models. From left to right and from top to bottom, climate variables are: near-surface air temperature (TAS in°C), sea level pressure (PSL in Pa), geopotential height (ZG500 in m) and vertical velocity at 500 hPa (WAP500 in Pa/s, positive values mean subsiding anomalies), surface downwelling shortwave and longwave radiation (RSDS and RLDS in W/m^2), latent and sensible heat flux (HFLS and HFSS in W/m^2), near-surface wind speed (WSPD in m/s), precipitation (PR in mm/d), total cloud fraction (CLT in %), and moisture in upper portion of soil column (MRSOS in kg/m^2).

changes simulated by LUCID-CMIP5 models largely agree on a deforestation signal in regions below 20°N, particularly in South America, South Africa, and southeastern Australia (see Figure 1). By contrast, models do not show a similar agreement in northern temperate or boreal regions: the models that do not include a dynamical representation of natural vegetation changes alongside anthropogenic disturbance (CanESM2 and IPSL-CM5A-LR) simulate a slight boreal deforestation while the other models including this dynamical representation (HadGEM2-ES, MPI-ESM-LR, and MIROC-ESM) exhibit an expansion of forest until 2100. The models agree however on a slight expansion of forest around western Europe and U.S. Midwest until 2100 (Figure S1 in the supporting information, black dots depict 100% agreement with respect to the sign of the anomaly among the five models). The implementation of LULCC in each model contributes to the spread in BPH projected changes that are discussed in section 4.

In order to analyze a wide range of future BPH responses to LULCC, 15 climate variables were selected (standard CMIP5 abbreviations are used; Table 1): skin temperature (TS), 2 m air temperature (TAS), precipitation (PR), sea level pressure (PSL), geopotential height at 500 hPa (ZG500), vertical velocity at 500 hPa (WAP500), surface downwelling shortwave and longwave radiative fluxes (RSDS and RLDS), surface upwelling shortwave and longwave radiative fluxes (RSUS and RLUS), sensible and latent heat

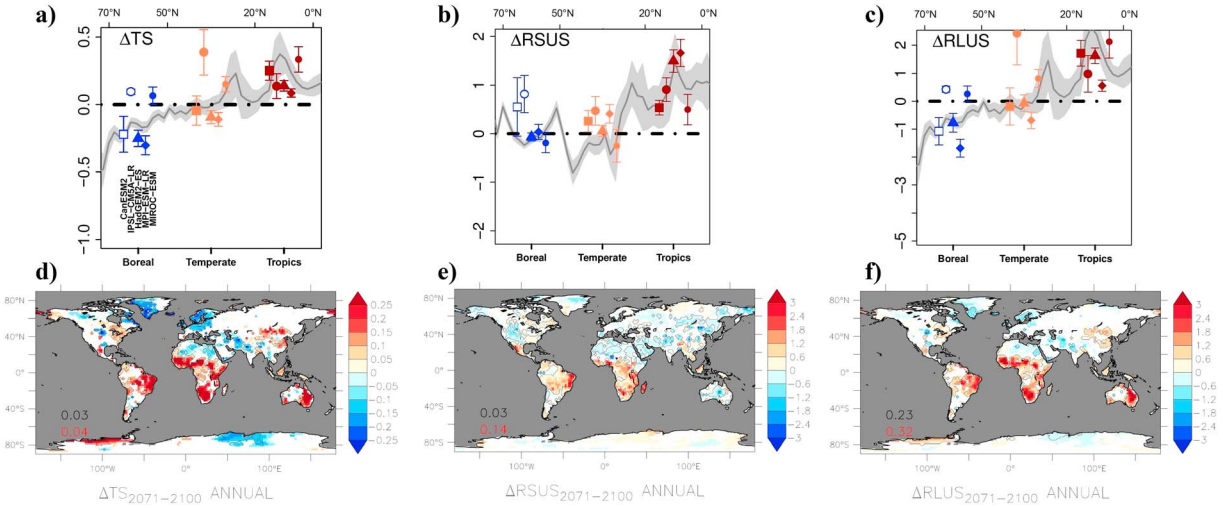

Figure 3. ENS-CMIP5 BPH changes in skin temperature (TS), surface upward shortwave, and longwave radiation (RSUS and RLUS). (a–c) Similar to Figure 2 but for TS, RSUS, and RLUS respectively. (d–f) Similar to Figure 4 but for TS (°C), RSUS (W/m^2), and RLUS (W/m^2).

flux (HFSS and HFLS), total cloud fraction (CLT), near-surface wind speed (WSPD, calculated as $\sqrt{\mathrm{UAS}^2 + \mathrm{VAS}^2}$ where UAS and VAS are the eastward and northward components of near-surface wind speed, respectively), and moisture in the upper portion of the soil column (MRSOS). Table 1 describes the availability of these variables among the models: 13 of these variables are available from all five models, while for the remaining two (WAP500 and MRSOS), outputs could only be retrieved for four models. "ENS-CMIP5" or ensemble-mean will refer to the average of BPH changes among all the available models. We investigate the climatic BPH responses induced by the future net changes in forest cover, assessing them for each model and above areas with different LULCC intensity (see Table S1 in the supporting information for the number of gridcells simulated by each model given some different ΔTreeFrac thresholds).

To assess likely impacts of future LULCC, we study here the significant BPH responses of the ensemble-mean changes. For regional ensemble averages and to estimate 95% confidence intervals, we use a Student's *t* test accounting for autocorrelation [*Zwiers and Von Storch*, 1995] (see grey curves and individual uncertainty bars in Figures 2 and 3a–3c). Additionally, BPH changes are found significant at grid cell scale when (i) at least 75% of the models agree on the sign of the ENS-CMIP5 anomaly (i.e., depending of model availability: at least, three models out of three, three models out of four, or four models out of five; see Table S1) and (ii) ENS-CMIP5 change is significant at the 95% level through a Mann-Whitney-Wilcoxon (MWW) test performed on 30 year simulations (RCP8.5 versus L2A85). Statistical significance in Figures 5 and 6 (black dots), 3d–3f, 4, and S2–S5 (black contours) is determined by the MWW test. This significance test is commonly used in regional climate studies [*Haensler et al.*, 2013; *Jacob et al.*, 2014; *Pfeifer et al.*, 2015] and has the advantage to not presume the distribution shape of a given variable [*Hollander and Wolfe*, 1999]. Normalized values in Figure 5 (seasonal BPH effects) are calculated with respect to mean and standard deviation of global annual ensemble-mean BPH changes on grid cells with $|\Delta\mathrm{TreeFrac}| > 5\%$, for each variable and each model. For Figure 6 (BPH sensitivity to LULCC intensity), normalized values are calculated with respect to mean and standard deviation of global annual ensemble-mean BPH changes, for each variable and each model. In order to assess relations between BPH effects and ΔTreeFrac, the *loess* package in R [*Cleveland et al.*, 1992] is used to fit locally weighted scatterplot smoothing and calculate the corresponding 95% confidence intervals (Figure 7). We also report and accordingly discuss as *low-representative* the ENS-CMIP5 values when some models simulate less than 50 gridcells in a region for a given LULCC threshold (empty dots in Figures 2 and 3 and dotted lines in Figure 7).

For the regional assessment, the BPH changes are calculated on continental grid points of three main climatic zones defined as "boreal" (latitude $\geq$ 50°N and $\leq$ 50°S), "temperate" (20°N $\leq$ latitude $\leq$ 60°N and 60°S $\leq$ latitude $\leq$ 20°S), and "tropics" (20°S $\leq$ latitude $\leq$ 20°N).

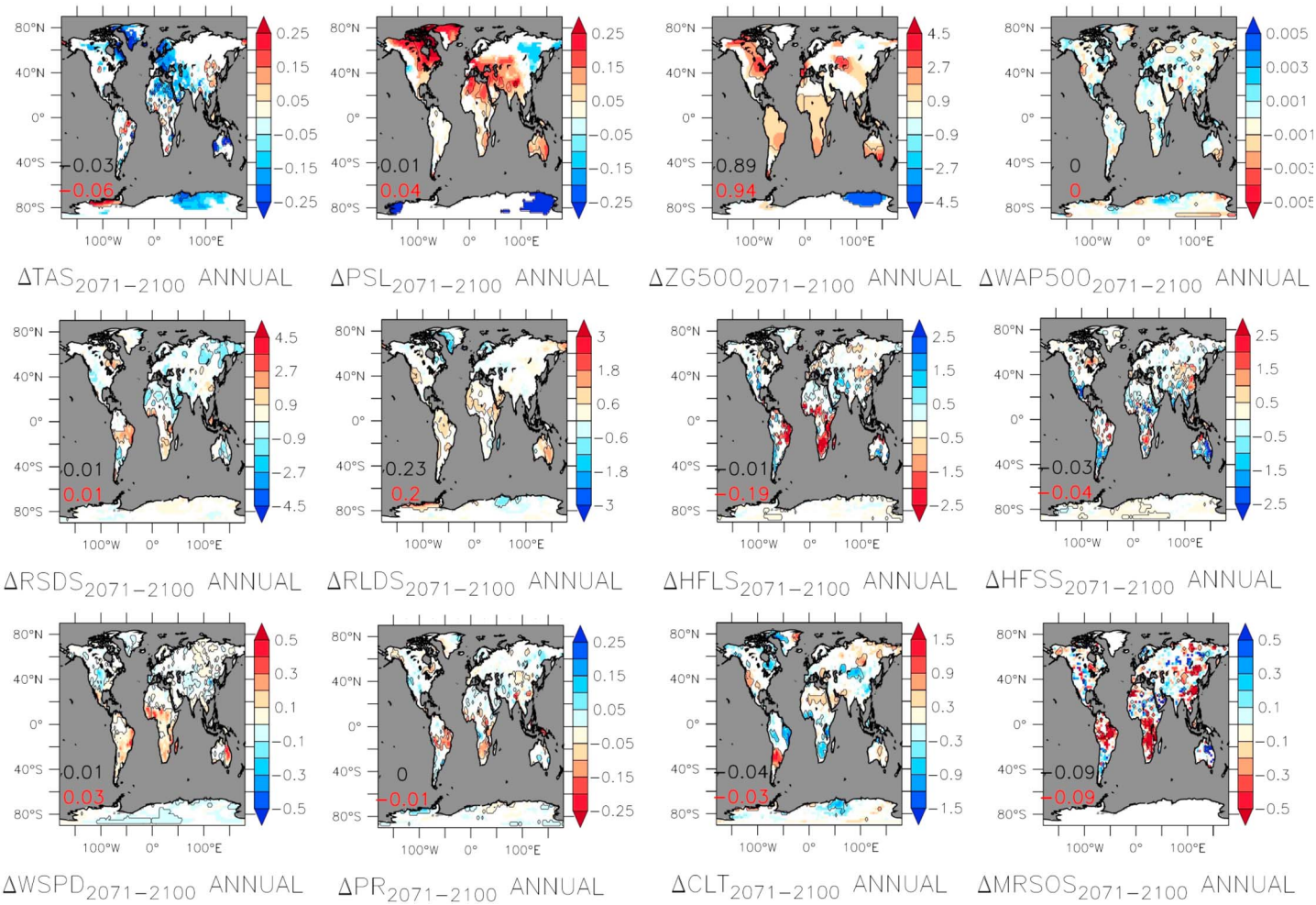

Figure 4. Spatial patterns of annual ENS-CMIP5 BPH changes in response to future LULCC for 2071–2100 (RCP8.5 scenario). Only continental grid points where at least 75% of the models have similar sign anomaly are displayed. The black contours depict regions where at least 75% of the models have similar sign anomaly, and the ensemble mean is significant at 0.05 level in a Mann-Whitney-Wilcoxon test. Ocean grid points are masked by grey shading. The black and red numbers in the bottom left corner indicate land + ocean and land-only averages for each variable changes, respectively.

3. Results

3.1. Large Climate Picture of Future LULCC-Biophysical Impacts

3.1.1. Effect on Atmospheric Variables

Figure 2 (top row) shows annual biophysical changes in TAS, PSL, ZG500, and WAP500 for areas with substantial future LULCC ($|\Delta\text{TreeFrac}| > 5\%$). On average, LULCC lead to small biophysical cooling in boreal and temperate regions of about −0.15°C and −0.08°C, respectively, while in the tropics, the change in TAS is zero on average (~0.0°C). Note that MIROC-ESM has a substantial BPH near-surface cooling response at global level, especially in tropics (~ −0.25°C), which is not the case for the other four models (see section 4.6 for the detailed model responses). However, all five models agree on an increase in skin temperature TS (+0.20°C on average; see Figure 3a). Zonal TAS changes for ENS-CMIP5 indicate cooling toward northern areas reaching up to −0.6°C around 70°N (Figure 2). This temperature gradient is even more pronounced for skin temperature TS (see Figures 3a and 3d). The IPSL-CM5A-LR model however differs in sign from the mean result showing slight near-surface warming in boreal (albeit with less than 10 gridcells; see Table S1) and temperate regions (+0.08°C and +0.12°C, respectively). Spatial patterns of BPH changes in annual temperatures are shown in Figure 4. BPH TAS cooling is found mainly located in northern Africa and southern Middle East (up to −0.3°C), Australia (up to −0.7°C), and northern Europe (up to −0.3°C). This biophysical cooling is slightly more pronounced above continental areas (−0.06°C) and above boreal areas with

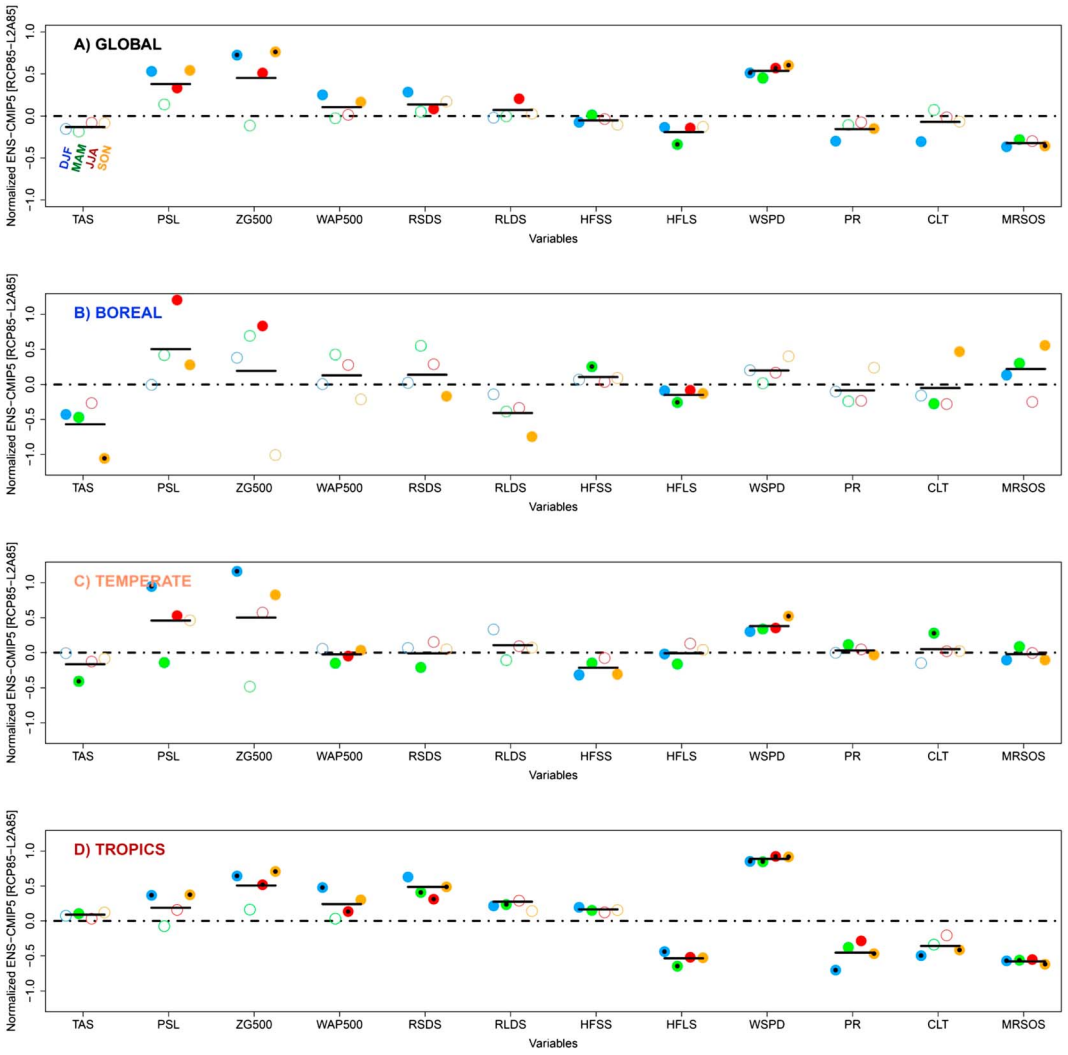

Figure 5. Normalized ENS-CMIP5 BPH changes for each season (winter, DJF; spring, MAM; summer, JJA; autumn, SON) (a) globally, (b) in the boreal regions, (c) in the temperate regions, and (d) in the tropics, for 2071–2100 (RCP8.5 scenario). Changes are averaged over grid points having experienced more than 5% change in tree fraction. For normalization of each variable and model response, the standard deviation of global annual BPH changes for $|\Delta\text{TreeFrac}| > 5\%$ is considered (see section 2). The *x* axis corresponds to each of the 12 climate variable considered. The filled colored circles represent ≥75% model agreement, and the black dots are added when values are also significant at 0.05 level through Mann-Whitney-Wilcoxon test. The annual normalized values are indicated for each variable by means of the black segments.

increase in tree cover (−0.09°C on areas with $\Delta\text{TreeFrac} > 0\%$) than globally (−0.03°C; see bottom left corners in Figure 4). Moreover, no significant biophysical near-surface warming occurs except in northern parts of Brazilian Amazon rainforest, of East Asia and of western Africa (0.1–0.2°C on annual average, enhanced in autumn; see Figure S5). By contrast, significant and robust skin temperature TS increases are found above tropical deforested areas like eastern South America, western and southern Africa, and eastern Australia, up to 0.6°C (see also section 4.2 for differences in the simulated TS and TAS responses; Figure 3d).

Surface pressure PSL increases significantly up to 0.3 hPa mainly in northern latitudes around northeastern America, northern Africa, and central Asia (Figure 4). These relatively higher pressures are co-located with denser air due to colder surface temperatures and are stronger on continental areas (+0.04 hPa for land versus +0.01 hPa for land + ocean; Figure 4). Models also simulate an increase in geopotential height ZG at 500 hPa of about 0.9 m globally and on land areas. This is robust among models in tropical areas, southern Australia and some temperate regions like northeastern U.S. The simulated changes in vertical velocity at 500 hPa (WAP500) are negligible at global level (0.0 Pa/s on average) but are significant in eastern

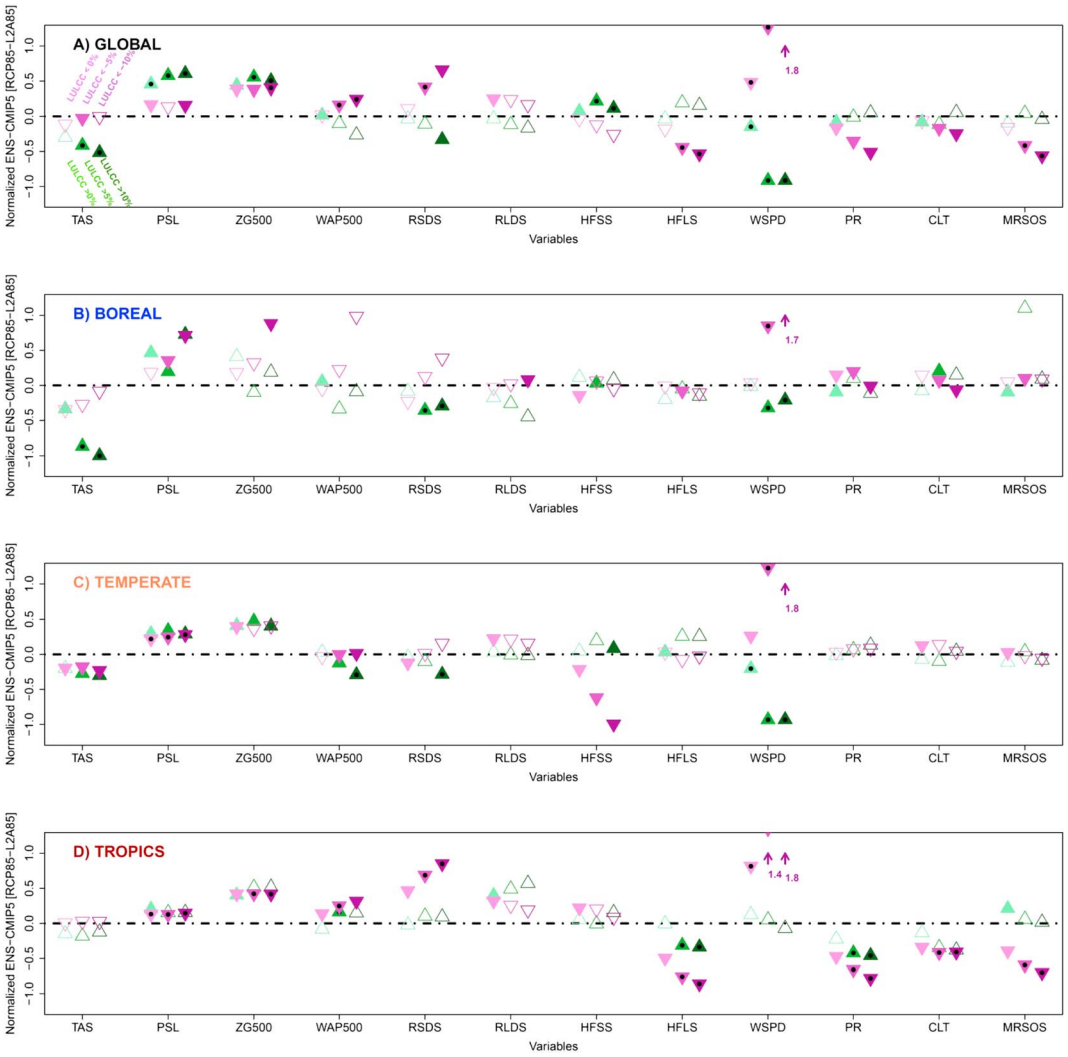

Figure 6. Normalized ENS-CMIP5 BPH changes for different ΔTreeFrac thresholds (in terms of 2100 minus 2006 tree fraction changes ΔTreeFrac: in green >0%, >5%, and >10% "re-afforested /afforested grid points" and in purple <0%, < −5%, and < −10% "deforested grid points") (a) globally, (b) in the boreal regions, (c) in temperate regions, and (d) in tropics, for 2071–2100 (RCP8.5 scenario). For normalization, the standard deviation of global annual BPH changes of each variable and each model is considered (see section 2). The *x* axis corresponds to each of the 12 climate variable considered. The filled colored triangles represent ≥75% model agreement, and the black dots are added when values are also significant at 0.05 level in a Mann-Whitney-Wilcoxon test. Note that some models are not represented when they do not simulate any gridcell satisfying ΔTreeFrac thresholds (see Table S1).

equatorial South America and Africa (+0.5 Pa/s on average, a positive sign being synonym of subsidence anomalies).

3.1.2. Effect on Heat Flux and Radiative Variables

Figure 2 (middle row) shows annual changes in heat fluxes and radiative variables (RSDS, RLDS, HFLS, and HFSS) for area with substantial future LULCC (|ΔTreeFrac| > 5%). In tropical regions, ENS-CMIP5 incoming shortwave and longwave downward radiations (RSDS and RLDS) increase by 1.0 W/m^2 and 0.3 W/m^2, respectively. Despite variability between models with respect to the sign of the response, all LUCID-CMIP5 models agree on an increase of the total incoming radiation (RSDS + RLDS) in tropical areas of |ΔTreeFrac| > 5% (+1.3 W/m^2 on average).

In the tropics, ENS-CMIP5 latent heat flux HFLS and sensible heat flux HFSS are responsive to LULCC with a decrease by 1.3 W/m^2 and a slight increase by 0.2 W/m^2, respectively. Around the Brazil region, models agree on decreases of HFLS and increases of HFSS (up to −4.8 W/m^2 and +3.8 W/m^2 locally, respectively; see

Figure 4), particularly during March-April-May (MAM) and September-October-November (SON) (see Figures S3 and S5). All models also agree on a decrease of the sum of these two heat fluxes (i.e., HFSS + HFLS) by -1.0 W/m^2 on average in tropics.

In parallel of those increased incoming radiation and decreased turbulent heat fluxes, all models simulate an increase of reflected solar radiation RSUS and an increase of upward longwave radiation RLUS, on average by +1.0 W/m^2 and 1.3 W/m^2, respectively (see Figures 3b and 3c).

In temperate regions, areas with $|\Delta\text{TreeFrac}| > 5\%$ exhibit on average decreases in HFSS but no conclusive changes for HFLS (Figure 2). However, similar to the tropics, all LUCID-CMIP5 models agree on a decline of turbulent fluxes (HFLS + HFSS) across deforested temperate regions. In boreal regions, ENS-CMIP5 changes in HFSS and HFLS are rather small: 0.3 W/m^2 and -0.3 W/m^2 on average, respectively (Figure 2).

We also find that for all models, substantially reforested areas ($\Delta\text{TreeFrac} > 5\%$) in temperate regions are cooler (TS differences of -0.21°K on average), with more turbulent heat fluxes (+1.70 W/m^2 for HFLS + HFSS) and less reflected solar radiation (-0.69 W/m^2 for RSUS) compared to substantially deforested areas ($\Delta\text{TreeFrac} < -5\%$) there (not shown).

3.1.3. Effect on Winds

LULCC has strong effects on wind speeds as reflected by WSPD patterns in Figures 2 and 4. All LUCID-CMIP5 models simulate an increase of 0.09 and 0.15 m/s on average, in temperate and tropical regions, respectively (Figure 2). Figure 4 shows wind speed increases up to +0.5 m/s mainly along the eastern coasts of the southern hemisphere continents (eastern Brazil, southeastern Africa, and eastern Australia) but also in western Africa. In temperate regions, wind speed increases are smaller than in the tropics. Temperate regions around 30°–50°N (e.g., U.S. Midwest, northern Africa, and some parts of western Europe) show WSPD decreases (up to ~ -0.15 m/s for zonal averages of ENS-CMIP5; Figure 2) while temperate regions around 20–30°N show WSPD increases (up to +0.15 m/s; Figure 2). In contrast, boreal regions do not respond with significant changes in wind speed due to future LULCC (Figures 2 and 4). At global scale, wind speeds are slightly increased by 0.03 m/s on land areas and by 0.01 m/s on land + ocean areas (Figure 4).

3.1.4. Effect on Hydrology

LULCC not only alter radiative, momentum, and energy balance but also the hydrological balance through changes in climate variables such as PR, MRSOS, and CLT (Figure 2, bottom row). ENS-CMIP5 shows a decrease in tropical annual precipitation of about -0.07 mm/d. Small parts of the Brazilian Amazon rainforest and of southern and western Africa indicate significant decreases in annual precipitation due to future LULCC (-0.1/-0.2 mm/d; Figures 2 and 4). However, changes in PR are not consensual among models in temperate and boreal regions (Figure 2). Global and land-only changes are close to zero (0 and -0.01 mm/d, respectively; Figure 4).

At annual scale, declines in soil-moisture MRSOS are found in the southern Amazon as well as in major parts of southern subtropical Africa and eastern China (an average tropical depletion of 0.35 kg/m^2 is found above substantially deforested areas). At global and continental scales, ENS-CMIP5 MRSOS decreases (-0.1 kg/m^2; Figure 4). This soil-moisture depletion is particularly marked in all models during June-July-August (JJA) season (Figure S4) in the above mentioned regions but also in continental Europe (up to -1 kg/m^2), Canada (up to -1 kg/m^2), Alaska (up to -0.8 kg/m^2), and eastern Asia (up to -1.1 kg/m^2).

With regard to cloud fraction changes, models simulate a decrease on average in tropical CLT (-0.4%). Significant decreases up to 1% are simulated across northern South America and southern Africa (Figure 4). There are also significant CLT increases simulated in western U.S. (~ +0.6% on average above significant areas), the desert regions of northern Africa (~0.4%), and the Southern Cone of South America (~1.0%).

3.2. Seasonal Biophysical Responses

Figure 5 summarizes the normalized responses of each biophysical variable to future LULCC above areas with substantial LULCC ($|\Delta\text{TreeFrac}| > 5\%$), for each season (December-January-February (DJF) in blue, MAM in green, JJA in red, and SON in yellow) and each climatic zone (in Figures 5a–5d). Interestingly, rather than temperature and precipitation, the most significant BPH responses among seasons are (i) increase in wind speed WSPD (all seasons, in temperate and tropical regions), (ii) increase in solar irradiance RSDS (in MAM and JJA in the tropics), and (iii) decrease of tropical latent heat flux HFLS (particularly in spring), clouds (in

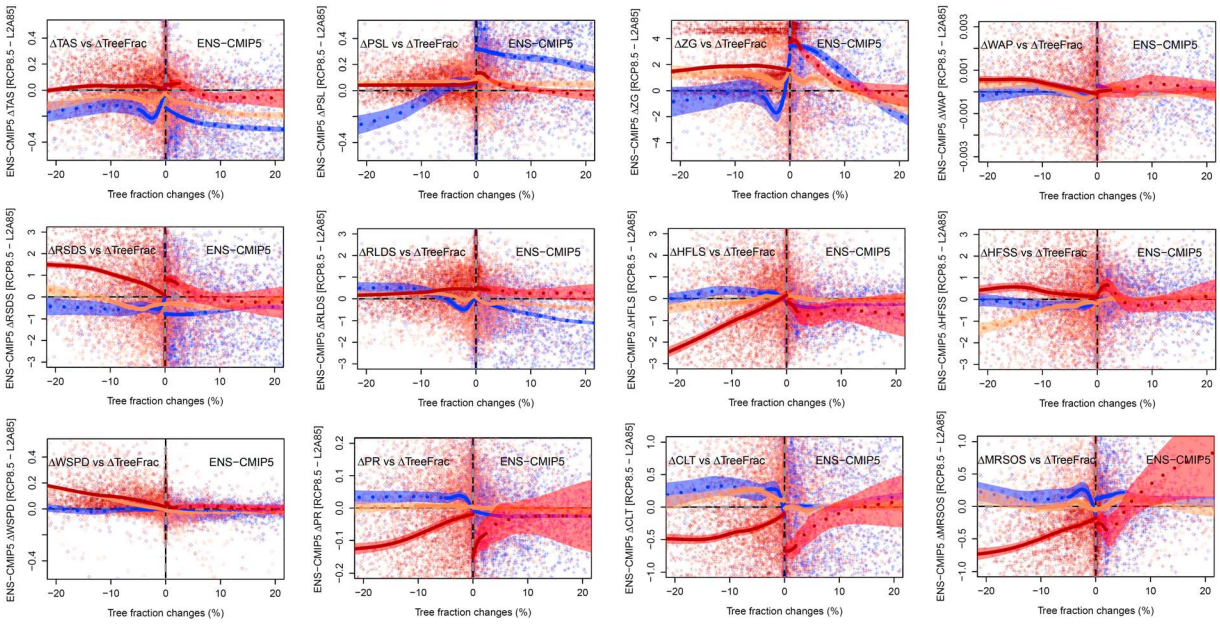

Figure 7. Relation between BPH changes in response to future LULCC (*y* axis) and tree fraction changes (*x* axis, between 2100 and 2006) for all grid points of the five LUCID-CMIP5 models together. For each variable, local polynomial regression fitting (LOESS fit curves) with 95% confidence-intervals for boreal (blue envelope), temperate (orange), and tropical (red) regions are displayed for ΔTreeFrac $>$ 0% and ΔTreeFrac $<$ 0% separately. The dotted (bold) curve portions indicate ΔTreeFrac ranges for which less than four models (all the five models) are available.

DJF and SON), and surface soil-moisture MRSOS (all seasons). Subsidence is also enhanced in the tropics during DJF and JJA (significant positive values for WAP500). Moreover, above areas with substantial land-use, all models agree on boreal biophysical cooling in autumn (SON). In DJF, concomitantly with deforested areas, the tropics display a significant perturbation of the hydrological cycle (Figure 5d): less soil moisture, less evaporation, and less precipitation and clouds (see section 4.4).

Highest variation among seasons is found for pressures variables (PSL/ZG500) reaching an intraannual 2 standard deviation in boreal region (Figure 5b). DJF and MAM seasons with 10 significant seasonal BPH responses are the most affected seasons and JJA the least affected.

3.3. Biophysical Response Versus LULCC Intensity

We investigate also the relationship between BPH responses and LULCC intensity for the main climatic zones. Figure 6 is similar to Figure 5 but analyzing BPH changes averaged on grid points with different degrees of LULCC (i.e., for ΔTreeFrac $>$0%, 5%, and 10% and for ΔTreeFrac $<$0%, $-$5%, and $-$10%). Note that the continuous relationship between local changes for each variable and ΔTreeFrac is displayed in Figure 7. The relationships between climate responses and LULCC intensity are nonlinear. In the majority of cases, when deforestation (Figure 6, purple triangles) increases in magnitude, BPH responses are amplified but much less when expansion of forest increases (green triangles).

In the tropics, for 12 out of 15 variables (TS, PR, PSL, ZG500, WAP500, RSDS, RSUS, RLUS, HFLS, CLT, WSPD, and MRSOS), the changes resulting from deforestation are significant if the LULCC perturbed area is larger than 5% (Figures 6d and S6). Tropical hydrological cycle is simulated to be significantly perturbed: rainfall, surface soil moisture, and cloudiness decrease with substantial deforestation. Surprisingly, rainfall and latent heat flux also decrease significantly above areas with expansion of forests (see Figure 6d; among the models, between 9 and 430 gridcells are affected by ΔTreeFrac $>$ 0%; see Table S1), but the magnitude of the changes is smaller and does not significantly change with the intensity of LULCC (see section 4.6).

In the temperate regions, irrespective of the sign and intensity of forest changes, a small biophysical cooling is simulated by four out of five LUCID-CMIP5 models (Figure 6c). On average, surface pressure and geopotential height (PSL and ZG500) are also showing positive changes independently of the sign and magnitude of forest changes. Other significant signals are detected: an increased subsidence, solar incoming and solar outgoing radiation (WAP500, RSDS, and RSUS) with increasing forest cover, and a strong negative

correlation between changes in wind speed WSPD and LULCC intensity (Figures 6c and S6g). In this climatic zone, nonsignificant responses of other variables are simulated.

In the boreal regions, we show that areas with increase (decrease) in tree cover tend to experience biophysical cooling (nonsignificant biophysical cooling, see TAS in Figure 6b). Other significant signals involve solar irradiance (RSDS) that decreases with local increase in forests larger than 5% and wind speed (WSPD) that increases with local deforestation (and decreases with expansion of forest; see Figure 5b). All other variable changes exhibit nonsignificant changes in the boreal region.

4. Discussion

With our analysis of the BPH impacts of future LULCC on 15 climate variables around 2071–2100 (RCP8.5 scenario) we aim to develop a wide multimodel climate picture of biophysical effects in response to a "reasonable" [*Pielke et al.*, 2011] future LULCC scenario, which substantially broadens previous analyses. Contrary to many studies focusing on one model or one idealized land cover change scenario, the BPH climate responses studied here represent the likely climatic impacts of a plausible future LULCC scenario applied to five different ESMs (Figure 1). As other added values, we disentangle results among models, seasons, latitudes, and LULCC intensity, bringing more physical elements to explain simulated BPH changes. We also consider here the net response to combined future LULCC, including both afforestation as well as deforestation, while most existing studies favor one or the other change. Note that we define "direct effects" as the biophysical effects due to LULCC implying changes in albedo, roughness, and evaporation efficiency, while "indirect effects" in response to LULCC describe the changes in, e.g., incoming solar radiation, incoming longwave radiation, air temperature, and humidity [e.g., *Chen and Dirmeyer*, 2016].

4.1. A Latitudinal Temperature Gradient

The latitudinal gradient of BPH effects on temperature previously put forward in the literature for regional or local complete deforestation [e.g., *Davin and de Noblet-Ducoudré*, 2010; *Lee et al.*, 2011] highlights opposite TAS responses to deforestation (respectively afforestation) between the tropics and boreal regions. This is also what we find here under future global LULCC scenario (from 0.1°C around the equator to −0.6°C around 70°N, on average above areas with substantial LULCC).

This gradient has been attributed to a gradual change in the relative contributions of evapotranspiration efficiency, roughness, and albedo contributions with latitude [*Davin and de Noblet-Ducoudré*, 2010]. Albedo changes tend to be negatively correlated with ΔTreeFrac, which are amplified by a snow-masking effect in winter in northernmost regions [*Betts*, 2000; *Lee et al.*, 2011; *Pitman et al.*, 2011; *Li et al.*, 2015]. The effects of evapotranspiration efficiency and roughness changes, usually opposite to the albedo effect, tend to be higher in tropical forests compared with temperate or boreal ones [*Bonan*, 2008; *Davin and de Noblet-Ducoudré*, 2010]. Although these direct effects can be important, we however find that indirect atmospheric processes could be dominant to explain the temperature changes in the boreal region (see section 4.6 and Text S1 in the supporting information).

The small global biophysical cooling simulated here (−0.03°C) has been found of similar magnitude in other studies that only deforested the tropics (−0.04°C on average globally [*Claussen et al.*, 2001; *Davin*, 2008; *Devaraju et al.*, 2015b; *Brovkin et al.*, 2015]). However, while we did not find a mean change in tropical surface air temperatures, we actually do find an increase in tropical skin temperature for all models (see section 4.2). Moreover, significant near-surface warming in the northwestern regions of the Brazilian Amazon or western Africa (up to 0.2°C; Figure 4) is more in line with previous studies considering local or regional tropical deforestation experiments [see, e.g., *Lejeune et al.*, 2014; *Lawrence and Vandecar*, 2015].

Global BPH temperature changes are similar to those found in studies accounting for historical LULCC ([*Pongratz et al.*, 2010]: −0.03/0.04°C for global and land-only averages; [*Davin et al.*, 2007]: −0.05°C) or future LULCC ([*Davin et al.*, 2007]: −0.14°C). Even if global BPH effects on temperature are small compared to all radiative forcings, future LULCC amplify on average the equator-to-pole temperature gradient calculated on areas with substantial LULCC ($|\Delta\text{TreeFrac}| > 5\%$), by 0.4°C annually with some seasonal modulation: 0.2°C only in JJA but 0.7°C in DJF. This modulation of the equator-to-pole temperature gradient is known to be associated with shifts in atmospheric features and poleward heat transport [*Lorenz*, 1984; *Marshall and Plumb*, 2007] which in turn affect substantially the regional climates (see section 4.5).

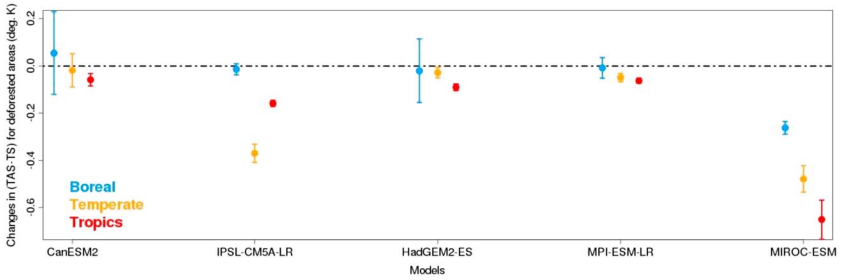

Figure 8. Changes in (TAS-TS) simulated above deforested areas (ΔTreeFrac $< 0\%$) in response to future LULCC, for each region (blue for boreal, orange for temperate, and red for tropics) and for each model (*x* axis). The uncertainty bars depict the 95% confidence intervals calculated on the basis of the spatial standard deviation and number of the relevant gridcells. Units: °K.

4.2. A Near-Surface Atmospheric Cooling Feedback

Figure 8 shows the changes in TAS − TS (near-surface air temperature minus skin temperature) for each model and each region above deforested areas (ΔTreeFrac $< 0\%$). We find that in temperate and tropics, all models simulate cooler near-surface atmospheric temperature than skin temperature above deforested areas (on average, -0.20°K in tropics for ΔTreeFrac $< -5\%$ at annual scale). This is also valid during all seasons and stronger for tropical and relatively bigger deforested areas (see Table S2).

This result is consistent with *Prigent* [2003], who found that greater skin-to-near-surface temperature gradient are consistent with more aerodynamic resistant land covers (e.g., crops versus forest), less soil moisture, and higher sensible heat flux. This result however is not clearly seen in observation studies as *Lee et al.* [2011] found no significant differences between changes in observed surface air and skin temperatures in open land versus in forested sites.

Note that MIROC-ESM, which simulates the strongest BPH cooling at global level (Figure S7), is also the model simulating the strongest near-surface cooling effect (TAS − TS) (Figure 8). This aspect deserves further investigation as reconstruction methods of direct effects of LULCC based on field observations or satellites (neglecting indirect effects in response to deforestation) could lead to systematic biases compared to global coupled simulations [*Perugini et al.*, 2017].

4.3. Strongest BPH Responses

Our study identifies that the strongest BPH responses to LULCC are simulated (i) in the tropics (namely, eastern South America, eastern Australia, and South Africa) and to a lesser extent in extratropical regions such as East Asia and eastern Canada, (ii) during DJF season, and (iii) for wind speed (WSPD, particularly in tropics and above deforested areas; Figure 6d). It appears also that stronger and more significant BPH responses are simulated over deforested areas than reforested ones (Figure 5).

WSPD changes are shown to have the highest sensitivity to LULCC as illustrated by Figures 6a–6d. Note that CMIP5 models simulate an increase of 0.04 m/s in globally averaged monthly wind speed [*Dobrynin et al.*, 2012] (RCP8.5–HIST, with HIST that corresponds to historical simulations in the 1950–2005 period). Our LUCID-CMIP5 analysis gives an increase of about 0.03 m/s over the continents in response to future LULCC. This may imply a large contribution of future tropical deforestation to projected trends in global continental wind speed. Caused by a reduced friction and a roughness length decrease, this strong and significant signal is fully consistent in magnitude with other studies [*Sud et al.*, 1996; *Schneider et al.*, 2006; *Vautard et al.*, 2010; *McVicar et al.*, 2012]. Based on mesoscale simulations of a regional coupled model, *Vautard et al.* [2010] claimed that roughness increase following increasing forest cover could have substantially (25–60%) led to observed northern hemisphere stilling in last 30 years (-0.3 m/s [*Bichet et al.*, 2012] or -0.4 m/s [*McVicar et al.*, 2012] in total for surface wind speeds). Our study shows that (i) regional near-surface wind speeds can be locally enhanced by +1 m/s per total forest removal in the temperate and tropical regions (sensitivity calculated on (-20% to 0%) ΔTreeFrac range; see also Figure 7 for ΔWSPD) but (ii) opposite LULCC signals in temperate regions lead to rather small decrease (-0.1 m/s) in near-surface wind speed around 30°–50°N. These results may have important implications for wind energy industry, air pollution modeling, and

erosion. Further coupled simulations with and without recent historical land use change would be needed to estimate the contribution of LULCC to regional wind speed trends and to separate these from other causes such as weakened equatorial-polar thermal gradient or large-scale circulation changes [*McVicar et al.*, 2012].

4.4. A Substantial Perturbation of the Hydrological Cycle

Our results also confirm findings previously obtained with LULCC scenarios or deforestation experiments that tended to show either nonsignificant [*Pitman et al.*, 2009; *de Noblet-Ducoudré et al.*, 2012; *Brovkin et al.*, 2013] or small reduction in global precipitation, mainly in the tropics [*Snyder*, 2004; *Bathiany et al.*, 2010; *Medvigy et al.*, 2010; *Lejeune et al.*, 2014; *Devaraju et al.*, 2015a]. Modest decreases simulated here over deforested areas of Amazon (up to −5% maximum; Figure 4) are however much lower than the reduction in precipitation in response to LULCC found in idealized deforested scenarios (roughly −15% or −1 mm/d in annual rainfall [*Lejeune et al.*, 2014; *Lawrence and Vandecar*, 2015]).

The relative decreases of tropical PR, MRSOS, CLT, and HFLS can be explained by the decrease in vegetation cover that further decreases transpiration as herbaceous vegetation tends to have shallower roots and less water interception [*Bonan*, 2008]. Decreases in latent heat flux HFLS above tropical deforested areas of -10 W/m^2 for complete deforestation are consistent with some literature values for Amazonian idealized deforestation (for example, -11.5 W/m^2 in *Lejeune et al.* [2014]) although values of -30 W/m^2 have also been found above the Amazon region [*Snyder*, 2010]. As soil moisture corresponds to the accumulation/depletion of precipitation minus evaporation minus runoff, we calculate that tropical MRSOS decreases (~ -0.3 kg/m^2) after tropical deforestation are more dominated by the precipitation decrease (-0.07 mm/d on average) than the evapotranspiration decrease (-0.04 mm/d) and the total runoff decrease (~ -0.01 mm/d, *mrro* CMIP5 variable). This explains in our simulations the soil-moisture depletion above tropical deforested areas.

Furthermore, the tropical soil-moisture depletions simulated in response to LULCC are comparable in magnitude to their projected changes induced by greenhouse gases under RCP8.5 scenario (see Figure 12.23 in *IPCC* [2013] with [−2; 2] kg/m^2 global minimum/maximal range of anomaly values). This clearly indicates that LULCC is a substantial and critical forcing for any hydrological assessment. As more than 25% of ESM do not include LULCC (see Table 12.1 in *IPCC* [2013]), their future regional projections for those variables are possibly biased and should be analyzed with caution. We not only confirm a perturbation of the hydrological cycle in the tropics (particularly in monsoon regions [*Quesada et al.*, 2016]) but also show significant MRSOS decreases in remote regions like Europe, East Asia, and United States especially during summer (see Figure S4).

In the same line, above temperate deforested areas, our multimodel framework simulates robust decreases in turbulent heat fluxes (HFLS + HFSS) for all models by ~1 W/m^2 (for ΔTreeFrac $< -5\%$) and ~0.3 W/m^2 (for ΔTreeFrac $< 0\%$) on average (not shown). This pattern confirms some temperate site-scale results [*Teuling et al.*, 2010; *Baldocchi and Ma*, 2013] but also contradicts others [*Schwalm et al.*, 2012], suggesting the sensitivity of this partitioning pattern to background climate, soil-moisture availability, and land cover transitions.

4.5. A Positive Tropical Soil-Moisture/Precipitation Feedback

LUCID-CMIP5 models draw the picture of a positive BPH tropical soil-moisture/precipitation feedback due to LULCC: when tropical deforestation increases (ΔTreeFrac decreases), less evaporation (HFLS) is simulated which implies less water vapor available to form clouds (CLT) which in turn (i) decreases local precipitation (PR) and (ii) increases incoming radiation (RLDS + RSDS). These two mechanisms increase the surface drying (less soil-moisture and precipitation). Figure 9 illustrates this "positive soil-moisture/precipitation feedback" picture showing large zones in tropical South America and Africa where this particular pattern is clearly simulated. This feedback is amplified by more anticyclonic conditions and increased subsidence in response to local tropical deforestation (Figure 6d for WAP and ZG500).

In the literature, the prevailing paradigm in tropics and Amazon region is a reduction of soil moisture in response to deforestation because of less precipitation, less rooting depth, and less water interception [*Pielke et al.*, 2011; *Lejeune et al.*, 2014; *Lawrence and Vandecar*, 2015]. This positive soil-moisture/precipitation feedback could have profound impacts, reducing agricultural yields [*Lawrence and Vandecar*, 2015], aggravating droughts [*Dirmeyer*, 1994], and heatwaves [*Quesada et al.*, 2012].

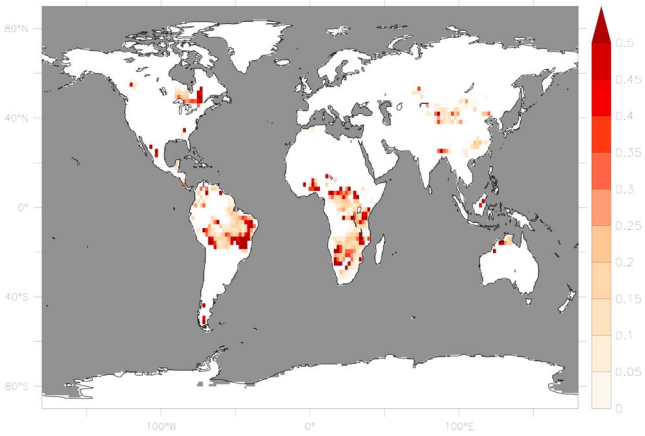

Figure 9. Coupling strength of "positive precipitation/soil-moisture feedback" after deforestation; i.e., ratio of annual BPH changes in PR by MRSOS (units: $\frac{mm/d}{kg/m^2}$) for deforested grid cells (ΔTreeFrac $< 0\%$) is displayed where all following conditions for ENS-CMIP5 values are met: precipitation (PR) decrease, latent heat flux (HFLS) decrease, total cloud fraction (CLT) decrease, soil-moisture (MRSOS) decrease, and total incoming radiation (RLDS + RSDS) increase.

Besides, a decent body of literature still debates the relation between LULCC and clouds following on from pioneering observational studies in Australia of *Lyons et al.* [1993] and *Lyons* [2002]. Both cloud responses have been documented: "more clouds above deforested areas" [*Chu et al.*, 1994; *Cutrim et al.*, 1995; *Gash and Nobre*, 1997; *Chagnon et al.*, 2004; *Negri et al.*, 2004; *Roy*, 2009; *Wang et al.*, 2009] and "less clouds above deforested areas" [*Lyons et al.*, 1993; *Sud et al.*, 1996; *Lawton et al.*, 2001; *Lyons*, 2002; *Sampaio et al.*, 2007; *Snyder*, 2010; *van der Molen et al.*, 2011; *Spracklen et al.*, 2012]. In tropical areas, our multimodeling study better supports on average the "less cloud above deforested areas" concept as displayed by Figure 9 and CLT/LULCC intensity relation in Figures 6d and 7. Our estimate is an ~3% decrease in total cloud fraction per total local deforestation in the tropics (calculation based on sensitivity for ΔTreeFrac in the range [-20%;0%] Figure 7). This pattern is also dependent on the scale of tropical deforestation that in the ESM and in the RCP8.5 is very large and widespread.

4.6. BPH Response Versus LULCC Intensity: Possible Remote Effects?

It is widely accepted that the impact of removing forests for agriculture depends on the spatial scale of the change [*Lawrence and Vandecar*, 2015; *Pitman and Lorenz*, 2016]. However, to our knowledge, few global studies addressed the linearity and strength of the relationship between BPH changes and LULCC intensity [e.g., *D'Almeida et al.*, 2007; *de Noblet-Ducoudré et al.*, 2012; *Wickham et al.*, 2013; *Badger and Dirmeyer*, 2015].

Observational studies [*Lee et al.*, 2011; *Zhang et al.*, 2014; *Li et al.*, 2015] and regional modeling experiments [*Bonan et al.*, 1992; *Betts*, 2000; *Claussen et al.*, 2001; *Snyder*, 2004; *Bala et al.*, 2007; *Bathiany et al.*, 2010; *Dass et al.*, 2013; *Devaraju et al.*, 2015b] show biophysical cooling under boreal deforestation and warming under boreal reforestation. Global, regional, or intermediate complexity climate models simulate biophysical cooling effect due to increased snow-masking albedo effect in the winter under a reduction of boreal forest cover. Other biophysical processes such as evapotranspiration efficiency and roughness length decreases after deforestation are thought to be dominated in this region by large increase in albedo [*Bonan*, 2008; *Davin and de Noblet-Ducoudré*, 2010]. For example, this expected boreal biophysical cooling can reach -0.8°C [*Claussen et al.*, 2001; *Bala et al.*, 2007] with even higher local responses that can exceed -4°C [*Devaraju et al.*, 2015b].

However, for four LUCID-CMIP5 models, the boreal TAS changes are opposite to the expected change due to LULCC: continental warming associated with boreal deforestation (CanESM2 and IPSL-CM5A-LR) and cooling associated with local expansion of forests (HadGEM2-ES and MPI-ESM-LR). MIROC-ESM simulates the strongest global biophysical cooling, for each region and during all seasons, above every subcategory affected by LULCC (ΔTreeFrac $< -5\%$, 0% and ΔTreeFrac $> 0\%$, 5%), indicating strong atmospheric and sea/ice feedback (see Text S1). Thus, in all cases, even if they are different, atmospheric and indirect feedback could explain the simulated boreal temperature changes. This tends to indicate a first clue to support the mechanism of indirect/remote LULCC effects on boreal climate, as discussed below.

In an attempt to quantify the relative sensitivity of temperature changes to different components of the surface energy balance, Figure 10 shows the relation between continental temperature BPH changes (TS for Figure 10a and TAS for Figure 10b; *x* axis) versus ΔRSDS + ΔRLDS, so-called "atmospheric feedback"; ΔRSUS-ΔRSDS, "solar reflection"; and ΔHFLS + ΔHFSS, "turbulent heat fluxes" (*y* axis). We find that surface temperature changes are more influenced by the atmospheric feedback through changes in incoming shortwave

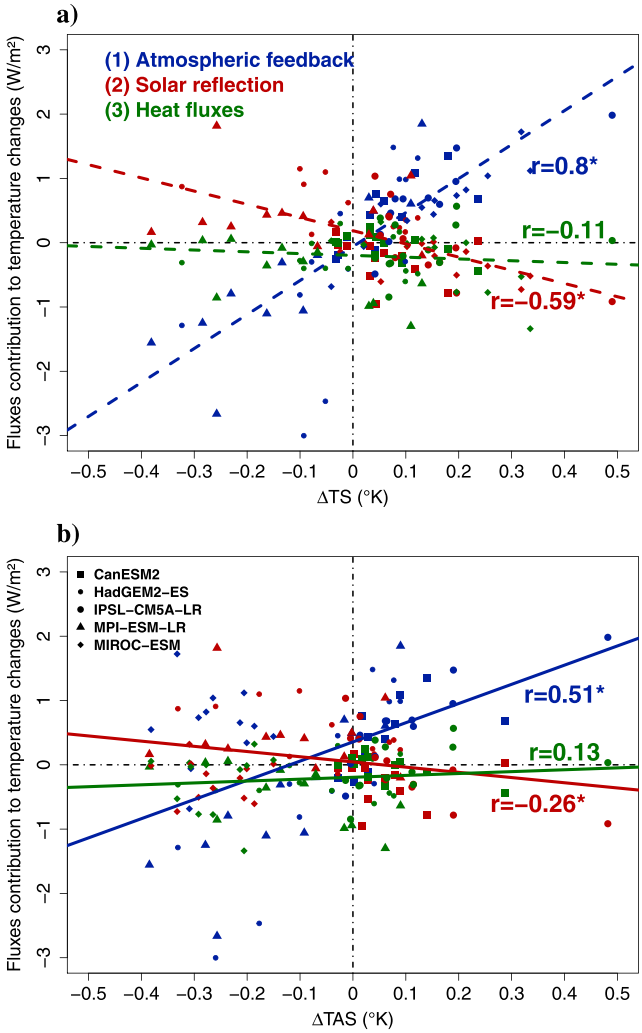

Figure 10. Fluxes contribution (W/m^2) to (a) skin and (b) surface air temperature changes (°K) on land areas. For each model (five different symbols), each season (DJF, MAM, JJA, and SON) and each region (boreal, temperate, and tropics), the relation between continental temperature BPH changes (*x* axis) versus ΔRSDS + ΔRLDS −(1) "atmospheric feedback" in blue–, ΔRSUS-ΔRSDS–(2) solar reflection in red–, and ΔHFLS + ΔHFSS −(3) heat fluxes in green–, is drawn (*y* axis). Linear trends and corresponding Pearson correlation coefficients values (*r*) are added for each contribution. A star symbol is added when the correlation is significant ($p < 0.05$).

and longwave (ΔRLDS + ΔRSDS) (r = +0.80/+0.51 for TS/TAS changes) than by solar reflection (ΔRSUS-ΔRSDS) (r = −0.59/−0.26) or heat fluxes (ΔHFLS + ΔHFSS) (r = −0.11/0.13 not significant), on average. Furthermore, on average when surface temperature is increased, solar reflection (negative fluxes contribution) is the physical process that tends to dampen the predominant atmospheric feedback (positive fluxes contribution; see Figures 10a and 10b and blue and red linear trends). Note that this behavior is common to the five LUCID-CMIP5 models: the relation atmospheric feedback versus TS changes is predominant (compared to "solar reflection" and "heat flux" contributions) with correlation ranges of [0.7; 0.9] among models. This relation is particularly marked in boreal (r = 0.82) and temperate regions (r = 0.76) compared to tropics (r = 0.52). In summary, our results show that, on average, indirect atmospheric effects of LULCC on temperature dominate over direct effects, particularly in boreal regions.

This could also be in accordance with an atmospheric mechanism put forward in the literature: tropical deforestation tends to dry the surface and the atmosphere (through less evaporative flux) and to increase of the top-of-the-atmosphere albedo, which can lead to tropospheric drying and cooling and modify the amount of atmospheric radiation that eventually leads to modulate boreal temperature changes, potentially enhanced by ocean and sea ice feedback [*Claussen et al.*, 2001; *Davin and de Noblet-Ducoudré*, 2010; *Snyder*, 2010]. Regional biophysical responses in temperatures are thus susceptible to be influenced by global changes driven by more dominant LULCC signal (e.g., tropical deforestation influence on boreal response).

A second clue for remote effects is that even for areas of negligible boreal LULCC, mean BPH changes are significantly different from 0. For instance, in Figure 7 for TAS at ΔTreeFrac ~0^+ and 0^-%, BPH temperature changes in boreal zones are significantly different from 0 for each model. This can be interpreted as an indirect temperature signal that is at work and particularly visible above regions with almost no LULCC. Moreover, boreal areas with ΔTreeFrac ~ 0^+ are significantly associated with positive anomalies of sea level pressures and geopotential heights at 500 hPa (blue curves for PSL and ZG500; Figure 7). Similarly, significant decreases in precipitation, soil moisture, and cloud fraction above tropical areas with ΔTreeFrac ~0^+ and 0^- tend to indicate also a remote pantropical signal that weakens the regional hydrological cycle (see also section 4.4).

Third, it is worth noting that grid cells in some regions exhibit a same sign of BPH response whatever the sign in tree fraction changes is. For instance, BPH temperature changes in temperate and boreal regions are negative above both deforested and reforested areas (see green and purple triangles for TAS Figure 6d). Likewise, decreases in tropical PR, HFLS, and CLT are simulated both above deforested and reforested areas (see green and purple triangles for these variables in Figure 6d). Furthermore, negligible changes of WSPD, MRSOS, and RSDS among tropical reforested areas are simulated despite a strong sensitivity of these variables to local LULCC intensity above deforested areas (Figure 6d). These observations indicate that the deforestation signals in the tropics have a biophysical influence that goes beyond the regions where the LULCC occur.

Finally, significant higher tropospheric geopotential (at 500 hPa) in the Northern Hemisphere (Figure 4) can also be caused by the presence of teleconnections that could lead, through changes in tropical energy balance, to significant tropospheric modulations in northern latitudes already reported by some studies [*Chase et al.*, 2000; *Werth and Avissar*, 2002; *Avissar and Werth*, 2005; *Snyder*, 2010; *Badger and Dirmeyer*, 2015; *Zhang et al.*, 2016]. Indeed, single model studies already suggested that LULCC could affect large-scale circulations through complex modifications of atmospheric winds, strength of Hadley and Ferrel cells [e.g., *Claussen et al.*, 2001; *Bathiany et al.*, 2010; *Davin and de Noblet-Ducoudré*, 2010; *Snyder*, 2010; *Devaraju et al.*, 2015a].

We stress that all calculations presented in this study have also been repeated by scaling every local biophysical change by the local changes in tree fraction (e.g., $\frac{\Delta TAS}{\Delta TreeFrac}$ with $|\Delta TreeFrac| > 5\%$, not shown). No gain in intermodel robustness is found which could mean that model disagreements in the sign of biophysical responses are marginally attributable to land cover maps spread among models. However, the magnitude of biophysical responses can be dependent on the absolute amount of deforestation [*Boisier et al.*, 2012]: we find that a majority of BPH responses are dampened when initial tree cover in 2006 is higher (i.e., relative changes in ΔTreeFrac versus TreeFrac in 2006 are small, not shown). We also tested here other LULCC thresholds (e.g., Figure 2 but with $|\Delta TreeFrac| > 10\%$, not shown), and results are essentially similar. One main reason to choose 5% rather than 10% threshold for the tree fraction changes is that no grid points in CanESM2 and very few in IPSL-CM5A-LR undergo such changes in boreal regions (Table S1). Snow amount, near-surface specific humidity, and runoff were initially studied here but their response to future LULCC is overall small and not significant.

5. Conclusion

This study assesses (i) a large set of climate variables together, (ii) with several global coupled models (i.e., model intercomparison exercise), and (iii) with global and plausible scenario of LULCC (i.e., RCP8.5). We find that models simulate a stronger latitudinal temperature gradient, a near-surface atmospheric cooling feedback, a significant weakening of the hydrological cycle, and a positive soil moisture/precipitation feedback, in response to future LULCC. Tropical changes in hydrological and momentum balances in response to future LULCC are comparable in magnitude to their future regional changes, which make LULCC an indispensable forcing to take into account in future climatic assessments. Our study reveals significant indirect atmospheric processes triggered by LULCC, implying substantial changes in incoming radiation, which dominate climatic responses over the direct effects. Our findings contribute to the understanding of the physical mechanisms triggered by LULCC and show that climate models are able to simulate some robust climate perturbations in response to LULCC. The physical mechanisms behind the indirect atmospheric processes are not apparent from the simulations and would need further investigation. We suggest that the LULCC-biophysical effects on climate are not strictly confined to the regions where the changes have occurred. Furthermore, as LULCC forcing could substantially differ, we recommend that in future assessment of multimodel experiments, scientists carefully differentiate climate models that do have dynamic vegetation from the ones that do not. This also means that future projections should take into account and assess the relative importance of biophysical direct and indirect effects of realistic LULCC scenarios.

Acknowledgments
This work is performed in the framework of the EC FP7 LUC4C project (http://luc4c.eu, grant 603542). The authors thank the data producers' from the LUCID-CMIP5 project (https://www.mpimet.mpg.de/en/science/the-land-in-the-earth-system/working-groups/climate-biogeosphere-interaction/lucid-cmip5/experiments/): Vivek Arora, Juan Pablo Boisier, Victor Brovkin, Patricia Cadule, Veronika Gayler, Etsushi Kato, Andy Pitman, Julia Pongratz, and Eddy Robertson, for producing and making available their model outputs and for their contribution. We also acknowledge the World Climate Research Programme's Working Group on Coupled Modelling, which is responsible for CMIP5 (http://cmip-pcmdi.llnl.gov/cmip5) and the climate modeling groups (listed in Table 1 of this paper). We thank the two anonymous reviewers who contributed to improve this manuscript. We finally want to deeply thank Pascal Yiou (LSCE) for his fruitful help in statistical analysis.

References

Alkama, R., and A. Cescatti (2016), Biophysical climate impacts of recent changes in global forest cover, *Science*, *351*(6273), 600–604, doi:10.1126/science.aac8083.

Anderson-Teixeira, K. J., P. K. Snyder, T. E. Twine, S. V. Cuadra, M. H. Costa, and E. H. DeLucia (2012), Climate-regulation services of natural and agricultural ecoregions of the Americas, *Nat. Clim. Change*, *2*(3), 177–181, doi:10.1038/nclimate1346.

Avissar, R., and D. Werth (2005), Global hydroclimatological teleconnections resulting from tropical deforestation, *J. Hydrometeorol.*, *6*(2), 134–145, doi:10.1175/JHM406.1.

Badger, A. M., and P. A. Dirmeyer (2015), Remote tropical and sub-tropical responses to Amazon deforestation, *Clim. Dyn.*, *1–10*, doi:10.1007/s00382-015-2752-5.

Bala, G., K. Caldeira, M. Wickett, T. J. Phillips, D. B. Lobell, C. Delire, and A. Mirin (2007), Combined climate and carbon-cycle effects of large-scale deforestation, *Proc. Natl. Acad. Sci. U.S.A.*, *104*(16), 6550–6555, doi:10.1073/pnas.0608998104.

Baldocchi, D., and S. Ma (2013), How will land use affect air temperature in the surface boundary layer? Lessons learned from a comparative study on the energy balance of an oak savanna and annual grassland in California, USA, *Tellus B*, *65*, doi:10.3402/tellusb.v65i0.19994.

Bathiany, S., M. Claussen, V. Brovkin, T. Raddatz, and V. Gayler (2010), Combined biogeophysical and biogeochemical effects of large-scale forest cover changes in the MPI earth system model, *Biogeosciences*, *7*(5), 1383–1399, doi:10.5194/bg-7-1383-2010.

Betts, R. A. (2000), Offset of the potential carbon sink from boreal forestation by decreases in surface albedo, *Nature*, *408*(6809), 187–190, doi:10.1038/35041545.

Bichet, A., M. Wild, D. Folini, and C. Schär (2012), Causes for decadal variations of wind speed over land: Sensitivity studies with a global climate model, *Geophys. Res. Lett.*, *39*, L11701, doi:10.1029/2012GL051685.

Boisier, J. P., N. de Noblet-Ducoudré, A. J. Pitman, F. T. Cruz, C. Delire, B. J. J. M. van den Hurk, M. K. van der Molen, C. Müller, and A. Voldoire (2012), Attributing the impacts of land-cover changes in temperate regions on surface temperature and heat fluxes to specific causes: Results from the first LUCID set of simulations, *J. Geophys. Res.*, *117*, D12116, doi:10.1029/2011JD017106.

Bonan, G. B. (2008), Forests and climate change: Forcings, feedbacks, and the climate benefits of forests, *Science*, *320*(5882), 1444–1449, doi:10.1126/science.1155121.

Bonan, G. B., D. Pollard, and S. L. Thompson (1992), Effects of boreal forest vegetation on global climate, *Nature*, *359*(6397), 716–718, doi:10.1038/359716a0.

Boysen, L. R., V. Brovkin, V. K. Arora, P. Cadule, N. de Noblet-Ducoudré, E. Kato, J. Pongratz, and V. Gayler (2014), Global and regional effects of land-use change on climate in 21st century simulations with interactive carbon cycle, *Earth Syst. Dyn.*, *5*(2), 309–319, doi:10.5194/esd-5-309-2014.

Bright, R. M. (2015), Metrics for biogeophysical climate forcings from land use and land cover changes and their inclusion in life cycle assessment: A critical review, *Environ. Sci. Technol.*, *49*(6), 3291–3303, doi:10.1021/es505465t.

Brovkin, V., et al. (2013), Effect of anthropogenic land-use and land-cover changes on climate and land carbon storage in CMIP5 projections for the twenty-first century, *J. Clim.*, *26*(18), 6859–6881, doi:10.1175/JCLI-D-12-00623.1.

Brovkin, V., T. Pugh, E. Robertson, S. Bathiany, C. Jones, and A. Arneth (2015), Cooling biogeophysical effect of large-scale tropical deforestation in three Earth System models, vol. B33F–06, Conference Paper 2015 AGU Fall Meeting.

Chagnon, F. J. F., R. L. Bras, and J. Wang (2004), Climatic shift in patterns of shallow clouds over the Amazon, *Geophys. Res. Lett.*, *31*, L24212, doi:10.1029/2004GL021188.

Chase, T. N., R. A. P. Sr, T. G. F. Kittel, R. R. Nemani, and S. W. Running (2000), Simulated impacts of historical land cover changes on global climate in northern winter, *Clim. Dyn.*, *16*(2–3), 93–105, doi:10.1007/s003820050007.

Chen, L., and P. A. Dirmeyer (2016), Adapting observationally based metrics of biogeophysical feedbacks from land cover/land use change to climate modeling, *Environ. Res. Lett.*, *11*(3), 034002, doi:10.1088/1748-9326/11/3/034002.

Chu, P.-S., Z.-P. Yu, and S. Hastenrath (1994), Detecting climate change concurrent with deforestation in the Amazon Basin: Which way has it gone?, *Bull. Am. Meteorol. Soc.*, *75*(4), 579–583, doi:10.1175/1520-0477(1994)075<0579:DCCCWD>2.0.CO;2.

Claussen, M., V. Brovkin, and A. Ganopolski (2001), Biogeophysical versus biogeochemical feedbacks of large-scale land cover change, *Geophys. Res. Lett.*, *28*(6), 1011–1014, doi:10.1029/2000GL012471.

Cleveland, W. S., E. Grosse, and W. M. Shyu (1992), Local regression models, *Stat. Models S*, *2*, 309–376.

Cutrim, E., D. W. Martin, and R. Rabin (1995), Enhancement of cumulus clouds over deforested lands in Amazonia, *Bull. Am. Meteorol. Soc.*, *76*(10), 1801–1805, doi:10.1175/1520-0477(1995)076<1801:EOCCOD>2.0.CO;2.

D'Almeida, C., C. J. Vörösmarty, G. C. Hurtt, J. A. Marengo, S. L. Dingman, and B. D. Keim (2007), The effects of deforestation on the hydrological cycle in Amazonia: A review on scale and resolution, *Int. J. Climatol.*, *27*(5), 633–647, doi:10.1002/joc.1475.

Dass, P., C. Müller, V. Brovkin, and W. Cramer (2013), Can bioenergy cropping compensate high carbon emissions from large-scale deforestation of high latitudes?, *Earth Syst. Dyn.*, *4*(2), 409–424, doi:10.5194/esd-4-409-2013.

Davin, E. L. (2008), Étude de l'effet biophysique du changement d'occupation des sols sur le système climatique, PhD thesis, from Université Pierre et Marie Curie (UPMC), presented on Avril, 29th 2008.

Davin, E. L., and N. de Noblet-Ducoudré (2010), Climatic impact of global-scale deforestation: Radiative versus nonradiative processes, *J. Clim.*, *23*(1), 97–112, doi:10.1175/2009JCLI3102.1.

Davin, E. L., N. de Noblet-Ducoudré, and P. Friedlingstein (2007), Impact of land cover change on surface climate: Relevance of the radiative forcing concept, *Geophys. Res. Lett.*, *34*, L13702, doi:10.1029/2007GL029678.

de Noblet-Ducoudré, N., et al. (2012), Determining robust impacts of land-use-induced land cover changes on surface climate over North America and Eurasia: Results from the first set of LUCID experiments, *J. Clim.*, *25*(9), 3261–3281, doi:10.1175/JCLI-D-11-00338.1.

Devaraju, N., G. Bala, and A. Modak (2015a), Effects of large-scale deforestation on precipitation in the monsoon regions: Remote versus local effects, *Proc. Natl. Acad. Sci.*, *112*(11), 3257–3262, doi:10.1073/pnas.1423439112.

Devaraju, N., G. Bala, and R. Nemani (2015b), Modelling the influence of land-use changes on biophysical and biochemical interactions at regional and global scales, *Plant Cell Environ.*, *38*, 1931–1946, doi:10.1111/pce.12488.

Dirmeyer, P. A. (1994), Vegetation stress as a feedback mechanism in midlatitude drought, *J. Clim.*, *7*(10), 1463–1483, doi:10.1175/1520-0442(1994)007<1463:VSAAFM>2.0.CO;2.

Dobrynin, M., J. Murawsky, and S. Yang (2012), Evolution of the global wind wave climate in CMIP5 experiments, *Geophys. Res. Lett.*, *39*, L18606, doi:10.1029/2012GL052843.

Gash, J. H. C., and C. A. Nobre (1997), Climatic effects of Amazonian deforestation: Some results from ABRACOS, *Bull. Am. Meteorol. Soc.*, *78*(5), 823–830, doi:10.1175/1520-0477(1997)078<0823:CEOADS>2.0.CO;2.

Haensler, A., F. Saeed, and D. Jacob (2013), Assessing the robustness of projected precipitation changes over central Africa on the basis of a multitude of global and regional climate projections, *Clim. Change*, *121*(2), 349–363, doi:10.1007/s10584-013-0863-8.

Hollander, M., and D. A. Wolfe (1999), *Nonparametric Statistical Methods*, 2nd ed., pp. 107–124, Wiley-Interscience, New York.

Intergovernmental Panel on Climate Change (IPCC) (2013), *Climate Change 2013: The Physical Science Basis. Contribution of Working Group I to the Fifth Assessment Report of the Intergovernmental Panel on Climate Change*, edited by T. F. Stocker et al., 1535 pp., Cambridge Univ. Press, Cambridge, U. K., and New York, doi:10.1017/CBO9781107415324.

Jacob, D., et al. (2014), EURO-CORDEX: New high-resolution climate change projections for European impact research, *Reg. Environ. Change*, *14*(2), 563–578, doi:10.1007/s10113-013-0499-2.
Lawrence, D., and K. Vandecar (2015), Effects of tropical deforestation on climate and agriculture, *Nat. Clim. Change*, *5*(1), 27–36, doi:10.1038/nclimate2430.
Lawton, R. O., U. S. Nair, R. A. Pielke, and R. M. Welch (2001), Climatic impact of tropical lowland deforestation on nearby montane cloud forests, *Science*, *294*(5542), 584–587, doi:10.1126/science.1062459.
Lee, X., et al. (2011), Observed increase in local cooling effect of deforestation at higher latitudes, *Nature*, *479*(7373), 384–387, doi:10.1038/nature10588.
Lejeune, Q., E. L. Davin, B. P. Guillod, and S. I. Seneviratne (2014), Influence of Amazonian deforestation on the future evolution of regional surface fluxes, circulation, surface temperature and precipitation, *Clim. Dyn.*, *44*(9–10), 2769–2786, doi:10.1007/s00382-014-2203-8.
Li, Y., M. Zhao, S. Motesharrei, Q. Mu, E. Kalnay, and S. Li (2015), Local cooling and warming effects of forests based on satellite observations, *Nat. Commun.*, *6*, 6603, doi:10.1038/ncomms7603.
Li, Y., N. De Noblet-Ducoudré, E. L. Davin, S. Motesharrei, N. Zeng, S. Li, and E. Kalnay (2016), The role of spatial scale and background climate in the latitudinal temperature response to deforestation, *Earth Syst. Dyn.*, *7*(1), 167–181, doi:10.5194/esd-7-167-2016.
Lorenz, E. N. (1984), Irregularity: A fundamental property of the atmosphere*, *Tellus A*, *36A*(2), 98–110, doi:10.1111/j.1600-0870.1984.tb00230.x.
Lorenz, R., and A. J. Pitman (2014), Effect of land-atmosphere coupling strength on impacts from Amazonian deforestation, *Geophys. Res. Lett.*, *41*, 5987–5995, doi:10.1002/2014GL061017.
Lyons, T. J. (2002), Clouds prefer native vegetation, *Meteorol. Atmos. Phys.*, *80*(1–4), 131–140, doi:10.1007/s007030200020.
Lyons, T. J., H. Xinmei, P. Schwerdtfeger, J. M. Hacker, I. J. Foster, and R. C. G. Smith (1993), Land–atmosphere interaction in a semiarid region: The bunny fence experiment, *Bull. Am. Meteorol. Soc.*, *74*(7), 1327–1334, doi:10.1175/1520-0477(1993)074<1327:LIIASR>2.0.CO;2.
Mahmood, R., et al. (2014), Land cover changes and their biogeophysical effects on climate, *Int. J. Climatol.*, *34*(4), 929–953, doi:10.1002/joc.3736.
Marshall, J., and R. A. Plumb (2007), *Atmosphere, Ocean and Climate Dynamics: An Introductory Text*, pp. 220–255, Academic Press, Cambridge, Mass.
McVicar, T. R., et al. (2012), Global review and synthesis of trends in observed terrestrial near-surface wind speeds: Implications for evaporation, *J. Hydrol.*, *416–417*, 182–205, doi:10.1016/j.jhydrol.2011.10.024.
Medvigy, D., R. L. Walko, and R. Avissar (2010), Effects of deforestation on spatiotemporal distributions of precipitation in South America, *J. Clim.*, *24*(8), 2147–2163, doi:10.1175/2010JCLI3882.1.
Negri, A. J., R. F. Adler, L. Xu, and J. Surratt (2004), The impact of Amazonian deforestation on dry season rainfall, *J. Clim.*, *17*(6), 1306–1319, doi:10.1175/1520-0442(2004)017<1306:TIOADO>2.0.CO;2.
Perugini, L., L. Caporaso, S. Marconi, A. Cescatti, B. Quesada, N. de Noblet, J. House, and A. Arneth (2017), Biophysical effects on temperature and precipitation due to land cover change, *Environ. Res. Lett.*, doi:10.1088/1748-9326/aa6b3f, in press.
Pfeifer, S., K. Bülow, A. Gobiet, A. Hänsler, M. Mudelsee, J. Otto, D. Rechid, C. Teichmann, and D. Jacob (2015), Robustness of ensemble climate projections analyzed with climate signal maps: Seasonal and extreme precipitation for Germany, *Atmosphere*, *6*(5), 677–698, doi:10.3390/atmos6050677.
Pielke, R. a., R. Avissar, M. Raupach, A. J. Dolman, X. Zeng, and A. S. Denning (1998), Interactions between the atmosphere and terrestrial ecosystems: Influence on weather and climate, *Global Change Biol.*, *4*(5), 461–475, doi:10.1046/j.1365-2486.1998.00176.x.
Pielke, R. A., et al. (2011), Land use/land cover changes and climate: Modeling analysis and observational evidence, *Wiley Interdiscip. Rev. Clim. Change*, *2*(6), 828–850, doi:10.1002/wcc.144.
Pitman, A. J., and R. Lorenz (2016), Scale dependence of the simulated impact of Amazonian deforestation on regional climate, *Environ. Res. Lett.*, *11*(9), 094025), doi:10.1088/1748-9326/11/9/094025.
Pitman, A. J., et al. (2009), Uncertainties in climate responses to past land cover change: First results from the LUCID intercomparison study, *Geophys. Res. Lett.*, *36*, L14814, doi:10.1029/2009GL039076.
Pitman, A. J., F. B. Avila, G. Abramowitz, Y. P. Wang, S. J. Phipps, and N. de Noblet-Ducoudré (2011), Importance of background climate in determining impact of land-cover change on regional climate, *Nat. Clim. Change*, *1*(9), 472–475, doi:10.1038/nclimate1294.
Pongratz, J., C. H. Reick, T. Raddatz, and M. Claussen (2010), Biogeophysical versus biogeochemical climate response to historical anthropogenic land cover change, *Geophys. Res. Lett.*, *37*, L08702, doi:10.1029/2010GL043010.
Prigent, C. (2003), Land surface skin temperatures from a combined analysis of microwave and infrared satellite observations for an all-weather evaluation of the differences between air and skin temperatures, *J. Geophys. Res.*, *108*(D10), 4310, doi:10.1029/2002JD002301.
Quesada, B., R. Vautard, P. Yiou, M. Hirschi, and S. I. Seneviratne (2012), Asymmetric European summer heat predictability from wet and dry southern winters and springs, *Nat. Clim Change*, *2*(10), 736–741, doi:10.1038/nclimate1536.
Quesada, B., N. Devaraju, N. de Noblet-Ducoudré, and A. Arneth (2016), Reduction of monsoon rainfall in response to past and future land-use and land-cover changes, *Geophys. Res. Lett.*, *44*, 1041–1050, doi:10.1002/2016GL070663.
Roy, S. B. (2009), Mesoscale vegetation-atmosphere feedbacks in Amazonia, *J. Geophys. Res.*, *114*, D20111, doi:10.1029/2009JD012001.
Sampaio, G., C. Nobre, M. H. Costa, P. Satyamurty, B. S. Soares-Filho, and M. Cardoso (2007), Regional climate change over eastern Amazonia caused by pasture and soybean cropland expansion, *Geophys. Res. Lett.*, *34*, L17709, doi:10.1029/2007GL030612.
Schneider, E. K., M. Fan, B. P. Kirtman, and P. A. Dirmeyer (2006) Potential effects of Amazon deforestation on tropical climate, *COLA Tech. Rep.*, *226*, 41 pp., Center for Ocean-Land Atmosphere Studies, Calverton, Md.
Schwalm, C. R., C. A. Williams, K. Schaefer, D. Baldocchi, T. A. Black, A. H. Goldstein, B. E. Law, W. C. Oechel, K. T. Paw U, and R. L. Scott (2012), Reduction in carbon uptake during turn of the century drought in western North America, *Nat. Geosci.*, *5*(8), 551–556, doi:10.1038/ngeo1529.
Snyder, P. K. (2004), Analyzing the effects of complete tropical forest removal on the regional climate using a detailed three-dimensional energy budget: An application to Africa, *J. Geophys. Res.*, *109*, D21102, doi:10.1029/2003JD004462.
Snyder, P. K. (2010), The influence of tropical deforestation on the northern hemisphere climate by atmospheric teleconnections, *Earth Interact.*, *14*(4), 1–34, doi:10.1175/2010EI280.1.
Spracklen, D. V., S. R. Arnold, and C. M. Taylor (2012), Observations of increased tropical rainfall preceded by air passage over forests, *Nature*, *489*(7415), 282–285, doi:10.1038/nature11390.
Sud, Y. C., W. K.-M. Lau, G. K. Walker, J.-H. Kim, G. E. Liston, and P. J. Sellers (1996), Biogeophysical consequences of a tropical deforestation scenario: A GCM simulation study, *J. Clim.*, *9*(12), 3225–3247, doi:10.1175/1520-0442(1996)009<3225:BCOATD>2.0.CO;2.
Teuling, A. J., et al. (2010), Contrasting response of European forest and grassland energy exchange to heatwaves, *Nat. Geosci.*, *3*(10), 722–727, doi:10.1038/ngeo950.

van der Molen, M. K., B. J. J. M. van den Hurk, and W. Hazeleger (2011), A dampened land use change climate response towards the tropics, *Clim. Dyn.*, *37*(9–10), 2035–2043, doi:10.1007/s00382-011-1018-0.

Vautard, R., J. Cattiaux, P. Yiou, J.-N. Thépaut, and P. Ciais (2010), Northern hemisphere atmospheric stilling partly attributed to an increase in surface roughness, *Nat. Geosci.*, *3*(11), 756–761, doi:10.1038/ngeo979.

van Vuuren, D. P., et al. (2011), The representative concentration pathways: An overview, *Clim. Change*, *109*(1–2), 5–31, doi:10.1007/s10584-011-0148-z.

Wang, J., F. J. F. Chagnon, E. R. Williams, A. K. Betts, N. O. Renno, L. A. T. Machado, G. Bisht, R. Knox, and R. L. Bras (2009), Impact of deforestation in the Amazon basin on cloud climatology, *Proc. Natl. Acad. Sci.*, *106*(10), 3670–3674, doi:10.1073/pnas.0810156106.

Werth, D., and R. Avissar (2002), The local and global effects of Amazon deforestation, *J. Geophys. Res.*, *107*(D20), 8087, doi:10.1029/2001JD000717.

Wickham, J. D., T. G. Wade, and K. H. Riitters (2013), Empirical analysis of the influence of forest extent on annual and seasonal surface temperatures for the continental United States, *Global Ecol. Biogeogr.*, *22*(5), 620–629, doi:10.1111/geb.12013.

Zhang, M., et al. (2014), Response of surface air temperature to small-scale land clearing across latitudes, *Environ. Res. Lett.*, *9*(3), 034002, doi:10.1088/1748-9326/9/3/034002.

Zhang, W., Z. Xu, and W. Guo (2016), The impacts of land-use and land-cover change on tropospheric temperatures at global and regional scales, *Earth Interact.*, *20*(7), 1–23, doi:10.1175/EI-D-15-0029.1.

Zwiers, F. W., and H. von Storch (1995) Taking Serial Correlation into Account in Tests of the Mean, *J. Clim.*, *8*(2), 336–351, doi:10.1175/1520-0442(1995)008<0336:TSCIAI>2.0.CO;2.